AIAA JOURNAL
Vol. 45, No. 7, July 2007

Trailing-Edge Flap Control of Dynamic Pitching Moment

P. Gerontakos* and T. Lee†
McGill University, Montreal, Quebec H3A 2K6, Canada

DOI: 10.2514/1.27577

The effects of upward ramp rate, actuation start time, and duration of a moveable trailing-edge flap on the critical aerodynamic values of an oscillating wing were investigated. The largest improvement in the peak negative pitching moment was obtained with a fast ramp rate and a start time near the mean angle. The largest value of net work coefficient, however, was generated with a delayed start time and a slower ramp rate. The peak lift coefficient decreased with increasing ramp rate and decreasing start time. The inclusion of a short steady-state portion in the flap motion was beneficial. An upward flap deflection initiated slightly after the mean angle during pitch-up, moved to its maximum deflection at a moderate speed, remained steady for a rather short period, and then returned to its initial position, which spanned half the oscillation cycle, was found to provide a best compromise between the various aerodynamic requirements.

Nomenclature

C_d	=	section drag coefficient
C_H	=	C_l hysteresis factor, $\int C_l(\alpha)\,\mathrm{d}\alpha$
C_l	=	section lift coefficient
C_m	=	section pitching moment coefficient
C_w	=	torsional damping factor or work coefficient
$C_{w,\mathrm{cw}}$	=	clockwise or negative C_w
$C_{w,\mathrm{ccw}}$	=	counterclockwise or positive C_w
$C_{w,\mathrm{net}}$	=	net C_w value, $C_{w,\mathrm{ccw}} + C_{w,\mathrm{cw}} = \int C_m(\alpha)\,\mathrm{d}\alpha = \int_{\mathrm{ccw}} C_m(\alpha)\,\mathrm{d}\alpha + \int_{\mathrm{cw}} C_m(\alpha)\,\mathrm{d}\alpha$
c	=	airfoil chord
f_o	=	oscillation frequency
Re	=	Reynolds number, $u_\infty c/\nu$
R1	=	upward flap deflection ramp rate
R2	=	downward flap deflection ramp rate
t	=	time
t_d	=	flap actuation duration
t_{R1}	=	flap upward deflection duration
t_s	=	flap actuation start time
t_{ss}	=	steady-state time period
u_∞	=	freestream velocity
x, y, z	=	streamwise, transverse, and spanwise distance
α	=	angle of attack
α_{ds}	=	dynamic-stall angle
α_m	=	mean angle of attack
$\alpha_{\max}$	=	maximum angle of attack
$\alpha_{\min}$	=	minimum angle of attack
α_{mp}	=	angle at $C_{m,\mathrm{peak}}$
$\Delta\alpha$	=	oscillation amplitude
$\delta_{\max}$	=	peak flap deflection
κ	=	reduced frequency, $\pi f_o c/u_\infty$
ν	=	kinematic viscosity
τ	=	phase angle, $2\pi f_0 t$

I. Introduction

THE dynamic overshoots in lift force and the accompanied high torsional and pitch control loads on retreating rotor blades continue to make dynamic stall and its control an important topic in rotorcraft engineering. The excessive aerodynamic loads of an oscillating airfoil, brought on by the formation, convection, and shedding of an energetic leading-edge vortex (LEV) are observed to result in some unwanted characteristics. These include a large degree of hysteresis in the lift coefficient, the severe nose-down pitching-moment coefficient seen as the LEV convects downstream over the airfoil, which leads to considerable pitch control loads, and the negative aerodynamic damping, which enhances vibrations. An excellent review on unsteady airfoils is given by McCroskey [1] and an in-depth experimental study on the characteristics of the unsteady boundary layer developed on oscillating airfoils is provided by Lee and Gerontakos [2].

In an attempt to minimize, or eliminate, the large hysteresis in the nonlinear airloads and the detrimental negative aerodynamic damping, numerous passive and active dynamic-stall flow control techniques (e.g., trailing-edge flaps [3–7], pulsating and synthetic jets [8,9], leading-edge blowing and suction [10], dynamically deformable leading edges [11], etc.) have been proposed. Among them, the trailing-edge flap (TEF) flow control method has been considered extensively by researchers to control the large nose-down pitching moment and/or negative damping induced on unsteady wings undergoing dynamic-stall oscillations, as well as for the control of the unsteady lift, including flutter suppression and gust alleviation. A representative numerical simulation of the TEF control of the pitching-moment loads associated with the dynamic stall occurring on a NACA 0012 airfoil, oscillated with $\alpha(t) = 15 + 10\sin 2\pi f_o t$ deg and a reduced frequency κ of 0.173 with $Re = 1.463 \times 10^6$, has been performed by Feszty et al. [6]. They found that the nose-down pitching moment could be reduced by the use of an optimum pulsed trailing-edge flap. Recently, the effect of a TEF deflection on the dynamic C_l and C_m loops, integrated from detailed surface pressure measurements, of a NACA 0015 airfoil, equipped with a dynamically deflecting 25% chord flap, oscillated with $\alpha(t) = 15 + 10\sin 2\pi f_o t$ deg and $\kappa = 0.05$ at $Re = 1.65 \times 10^5$ were documented by Gerontakos and Lee [7]. Similar to the pulsed flap motion employed by Feszty et al. [6], the first-harmonic TEF actuation consisted of a brief pulse, represented by a constant ramp-up motion, remained steady briefly, and was followed by a constant ramp-down motion. The prescheduled TEF motions were actuated at start times $t_s = -0.5\pi$, 0π, and 0.5π (corresponding to a flap actuation at $\alpha_{\min}$, α_m, and $\alpha_{\max}$, respectively) with $\delta_{\max} = \pm 7.5$ deg and ± 15 deg, and $t_d = 35$–$50\% f_o^{-1}$. Despite the limited control of the flap deflection waveform, general guidelines for choosing the various parameters describing the flap deflection (i.e., start time t_s, deflection duration t_d, and deflection magnitude $\delta_{\max}$) were suggested by Gerontakos and Lee [7]. They concluded that 1) the larger the upward $\delta_{\max}$, the more efficient the negative $C_{m,\mathrm{peak}}$ reduction mechanism; 2) the shorter the t_d, the smaller the poststall lift loss; 3) the magnitudes of maximum C_l and C_d seemed to be

Received 29 August 2006; revision received 19 January 2007; accepted for publication 13 February 2007.

*Graduate Research Assistant, Department of Mechanical Engineering.
†Associate Professor, Department of Mechanical Engineering. Member AIAA.

somewhat insensitive to the extent of flap actuation duration but were of lower values than a baseline, or uncontrolled, airfoil; 4) the later the t_s, the larger the net torsional damping factor, in general; and 5) the leading-edge vortex formation and detachment were not affected by the TEF motion; however, the low pressure signature or footprint of the LEV was reduced by the upward flap deflection. More important, the reduction in $|C_{m,\text{peak}}|$ was found to be mainly a consequence of the suction pressure introduced on the lower surface of the control flap.

The objective of this study was to extend the previous work of Gerontakos and Lee [7] to investigate the pronounced effect of the flap deflection ramp rate on the critical aerodynamic values via a newly integrated TEF control system with improved controllability. A parametric study was conducted that had as parameters the start time (between the mean and maximum angles of attack during the upstroke), deflection duration (30, 50, and 70%), ratio of steady-state deflection to total deflection (0 and 50%), and the flap deflection rates (chosen based on the t_{ss}/t_d and the limits of the mechanical system). These were then used to determine a best-possible flap deflection motion based upon the desired effects on the various performance characteristics.

II. Experimental Methods

The experiment was conducted in the suction-type wind tunnel at McGill University. The NACA 0015 wing, equipped with a full-span 25%c TEF, was oscillated beyond its static-stall angle of 18 deg with $\alpha(t) = 16 + 8\sin 2\pi f_o t$ deg and $f_o = 1.88$ Hz or $\kappa = 0.1$ (Fig. 1a). A u_∞ of 15 m/s and a chord of 25.4 cm resulted in $Re = 2.46 \times 10^5$. The surface pressure distributions were obtained from 48 0.35-mm-diam pressure taps, covering up to $x/c = 96.3\%$, distributed over the upper and lower surfaces of the wing model (Fig. 1b). The TEF, triggered in response to the oscillating airfoil phase angle τ, was actuated by a Maxon servomotor (model Re-35), incorporating a 4.3:1 helical gearbox and an optical encoder. The flap motion, described by the time of TEF initial deflection (i.e., start time t_s), the upward ramp rate R1, peak deflection amplitude $\delta_{\max}$, steady-state motion t_{ss}, downward ramp rate R2, and total deflection time t_d, was controlled by a Maxon EPOS 70/10 programmable motion controller. A more detailed description of the experimental setup is given by Gerontakos and Lee [7]. Note that when the phase angle was within the range $-0.5\pi \le \tau \le 0.5\pi$, the wing was described to be in pitch-up; when $0.5\pi \le \tau \le 1.5\pi$, the wing was said to be in pitch-down.

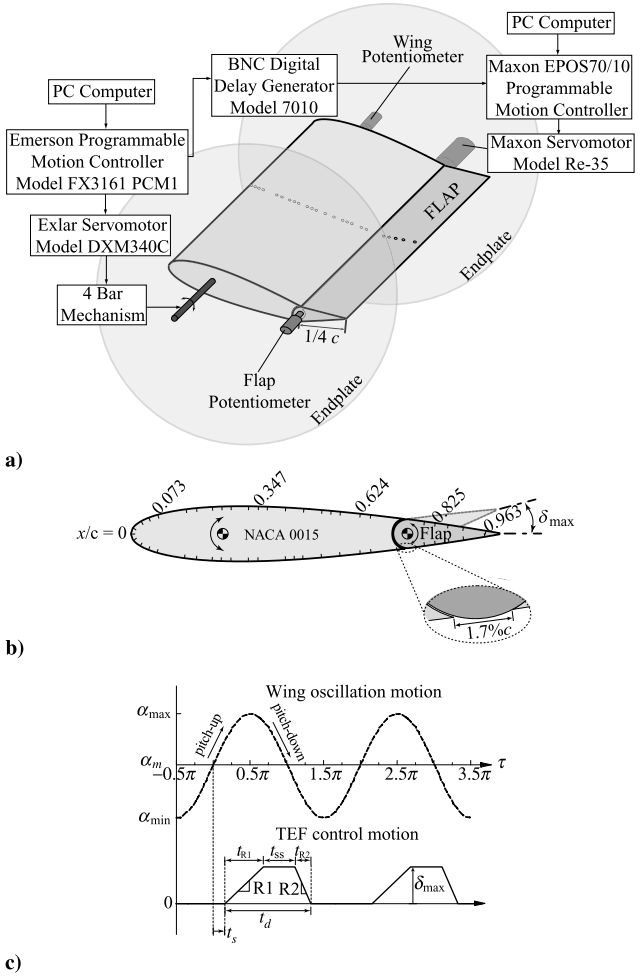

Fig. 1 a) Schematic of wing model and actuation mechanisms, b) pressure orifice locations, and c) TEF motion profile.

III. Results and Discussion

A. Effect of t_s and t_d

To further examine the effects of the upward flap deflection start time t_s ($= -0.5\pi$, 0π, and 0.5π corresponding to $\alpha = \alpha_{\min}, \alpha_m$, and $\alpha_{\max}$ during the pitch-up motion) and duration t_d ($\approx$30, 50, and $70\% f_o^{-1}$), with R1 = R2 fixed at about $11\% f_o^{-1}$ and $\delta_{\max}$ set to 16 deg ($=67\%\alpha_{\max}$), on the dynamic load curves, the variation of the critical aerodynamic values, such as $C_{l,\max}$, $C_{m,\text{peak}}$, $C_{w,\text{net}}$, $|C_{l,\max}/C_{m,\text{peak}}|$, and C_H, with t_d at different t_s, was characterized first and is presented in Fig. 2. Also shown in Fig. 2 are the baseline, or uncontrolled, airfoil data. The critical aerodynamic values and the TEF motion profiles are tabulated in Table 1.

Figure 2a demonstrates that the $C_{m,\text{peak}}$ requires a t_s before the occurrence of moment stall, irrespective of t_d, because an improvement is only seen for $t_s < 0.28\pi$. A linear reduction in $|C_{m,\text{peak}}|$, compared to a baseline airfoil, with increased t_d was observed for $t_s = -0.5\pi$ (or a flap deflected at $\alpha_{\min}$); the longer the flap actuation, the less the peak nose-down pitching moment. This resulted from a transition from undeflected to fully deflected flap position as t_d increased at the instant when the LEV was traveling downstream over the airfoil. At $t_s = 0\pi$ (corresponding to an upward deflection at α_m during pitch-up), a consistent improvement of about 40% in $C_{m,\text{peak}}$, effectively insensitive to t_d, was exhibited as a result of the coincidence of the peak flap deflection with the occurrence of moment stall. It can therefore be concluded that t_s should occur before moment stall, and that any t_s below 0π requires a reasonably long t_d. The details of the dynamic C_m–α loops at $t_s = 0\pi$ with $t_d \approx 30$, 50, and $70\% f_o^{-1}$ are presented in Figs. 3a–3c and show the significant reduction in $C_{m,\text{peak}}$ that is obtained regardless of t_d for a deflection beginning at the mean angle.

In contrast to the virtually unchanged $C_{m,\text{peak}}$, Fig. 2b indicates that the $t_s = 0.5\pi$ control case persistently provided a significant increase (0.52 to 1.27 compared to -0.16 for a baseline airfoil) in $C_{w,\text{net}}$ (see Table 1); the largest of any t_s regardless of t_d. This is a direct consequence of a significant suction pressure on the flap lower side, which persists solely during the downstroke, resulting in nose-up pitching moment and contributing to $C_{w,\text{ccw}}$. On the other hand, the $t_s = -0.5\pi$ case presented an increased $|C_{w,\text{cw}}|$ resulting in a considerably reduced $C_{w,\text{net}}$ compared to a baseline airfoil, as a result of an increased/unchanged C_m during the upstroke/downstroke (except for the longest duration), which translates into slightly smaller counterclockwise loops but significantly larger clockwise loops. Note that a counterclockwise C_m loop gives rise to a positive, or $C_{w,\text{ccw}}$, value whereas a clockwise C_m renders a negative, or $C_{w,\text{cw}}$, value. The results for $t_s = 0\pi$ fall in between the other two start times and show a linear increase in $C_{w,\text{net}}$ with t_d as the flap loading extends more into the downstroke; the $C_{w,\text{net}}$ was above the baseline airfoil value for $t_d \ge 50\% f_o^{-1}$. Figure 2b therefore implies that for an improved aerodynamic damping, a $t_d < 50\% f_o^{-1}$ requires a minimum t_s slightly after 0π (i.e., the smaller the t_d the later the t_s required) and a $t_d > 50\% f_o^{-1}$ allows a minimum t_s slightly earlier than $t_s = 0\pi$. A minimum allowable t_s just around $t_s = 0\pi$ is consequently preferred. Note that the effectiveness of the trailing-edge flap to manipulate the pitching moment and thus control the aerodynamic damping is demonstrated in Figs. 3a–3c. In particular,

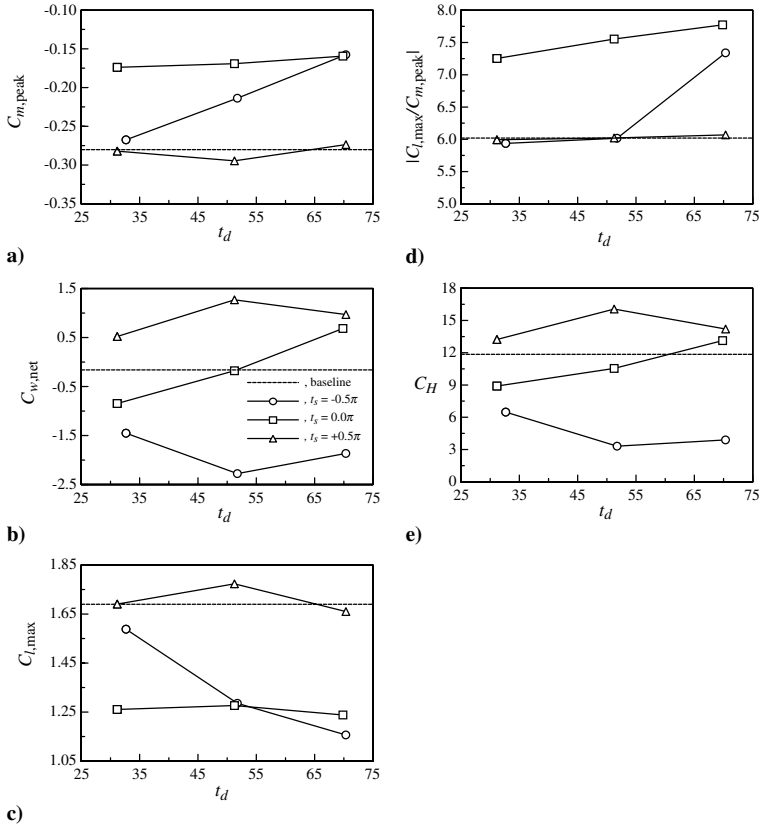

Fig. 2 Critical aerodynamic values for various t_d and t_s.

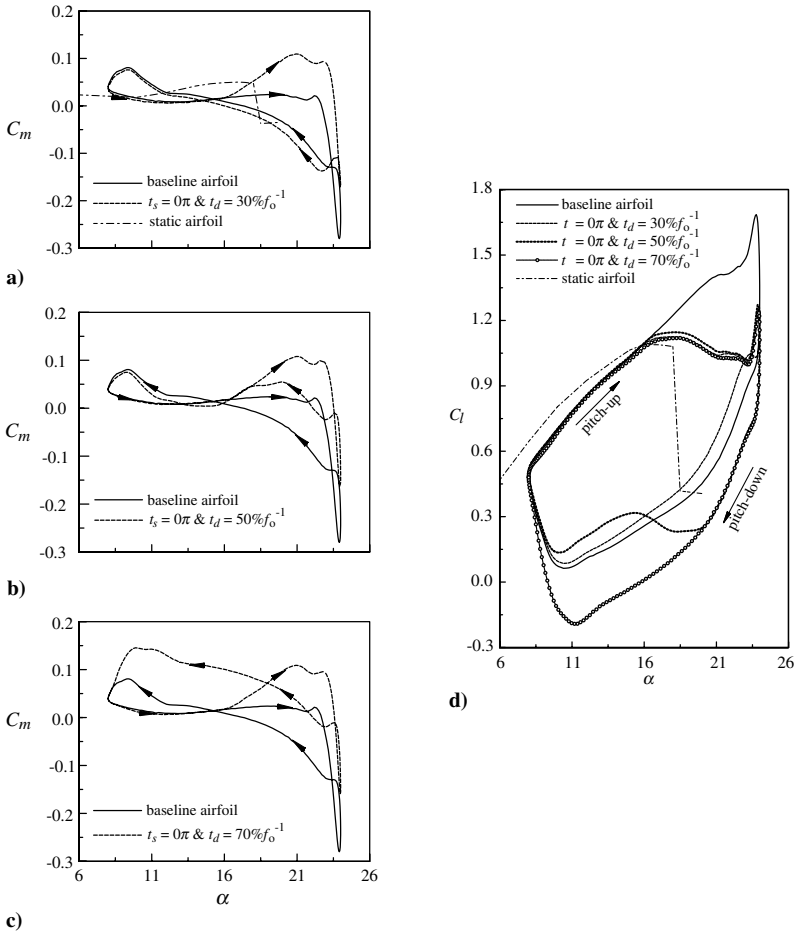

Fig. 3 Dynamic C_m and C_l loops for $\delta_{\max} = 16$ deg.

Table 1 TEF motion profiles and critical aerodynamic values

	t_s	t_d, %	t_{ss}/t_d	t_{R1}, %	t_{R2}, %	$C_{l,\max}$	α_{ds}, deg	$C_{m,peak}$	α_{mp}, deg	$\lvert C_{l,\max}/C_{m,peak}\rvert$	$C_{w,ccw}$	$C_{w,cw}$	$C_{w,net}$	C_H
Baseline airfoil						1.69	23.8	−0.280	23.9	6.02	0.25	−0.41	−0.16	11.9
$\delta = 16$ deg (static flap)						1.22	23.9	−0.170	24.0	7.19	0.26	−0.41	−0.15	9.8
1	-0.50π	32.7	0.29	11.6	11.6	1.59	23.8	−0.267	23.9	5.94	0.03	−1.48	−1.45	6.5
2	0.00π	31.2	0.31	10.1	11.6	1.26	23.9	−0.174	24.0	7.25	0.19	−1.03	−0.85	8.9
3	0.47π	31.2	0.29	11.6	10.6	1.69	23.8	−0.282	23.9	5.99	0.55	−0.03	0.52	13.2
4	-0.47π	51.8	0.57	11.6	10.6	1.29	24.0	−0.214	24.0	6.02	0.01	−2.29	−2.28	3.3
5	0.00π	51.3	0.55	11.6	11.6	1.28	23.9	−0.169	24.0	7.55	0.17	−0.34	−0.18	10.5
6	0.46π	51.3	0.56	11.6	11.1	1.77	23.8	−0.295	23.9	6.02	1.30	−0.03	1.27	16.1
7	-0.47π	70.3	0.69	11.6	10.6	1.16	23.9	−0.158	24.0	7.34	0.01	−1.88	−1.87	3.9
8	0.00π	69.9	0.67	11.6	11.6	1.24	23.9	−0.159	24.0	7.77	0.99	−0.31	0.68	13.1
9	0.46π	70.4	0.69	10.6	11.6	1.66	23.8	−0.274	23.9	6.07	0.99	−0.02	0.97	14.2
10	0.00π	51.3	0.00	10.1	41.2	1.27	24.0	−0.165	24.0	7.70	0.19	−0.78	−0.59	9.9
11	0.00π	49.8	0.00	13.1	36.7	1.30	23.9	−0.184	23.9	7.07	0.21	−0.67	−0.46	10.4
12	0.00π	51.3	0.00	25.6	25.6	1.42	23.8	−0.193	23.9	7.36	0.24	−0.37	−0.13	11.5
13	0.00π	51.3	0.00	38.2	13.1	1.49	23.8	−0.218	23.9	6.84	0.27	−0.08	0.19	12.3
14	0.00π	51.3	0.00	42.7	8.5	1.56	23.8	−0.232	23.9	6.73	0.37	−0.10	0.27	12.6
15	0.12π	52.8	0.00	8.5	44.2	1.30	23.8	−0.179	23.9	7.27	0.27	−0.38	−0.11	11.5
16	0.12π	52.8	0.00	13.6	39.2	1.35	23.8	−0.180	23.9	7.53	0.27	−0.30	−0.03	11.8
17	0.12π	51.8	0.00	25.6	26.1	1.55	23.8	−0.226	23.9	6.85	0.37	−0.08	0.29	12.6
18	0.12π	49.8	0.00	36.7	13.1	1.57	23.8	−0.243	23.9	6.46	0.59	−0.08	0.51	13.3
19	0.12π	51.2	0.00	41.2	10.0	1.61	23.8	−0.246	23.9	6.55	0.73	−0.09	0.64	13.5
20	0.25π	52.8	0.00	9.5	43.2	1.47	23.6	−0.207	23.9	7.09	0.51	−0.09	0.43	13.1
21	0.25π	51.3	0.00	13.1	38.2	1.56	23.6	−0.229	23.8	6.82	0.58	−0.05	0.53	13.6
22	0.25π	51.3	0.00	25.6	25.6	1.66	23.6	−0.258	23.9	6.45	0.78	−0.02	0.76	14.3
23	0.25π	51.3	0.00	37.7	13.6	1.68	23.6	−0.269	23.9	6.23	1.00	−0.07	0.93	14.8
24	0.25π	51.3	0.00	41.2	10.1	1.69	23.7	−0.271	23.9	6.22	1.03	−0.09	0.94	15.0
25	0.00π	49.8	0.50	8.5	16.1	1.14	23.9	−0.151	24.0	7.54	0.17	−0.62	−0.46	10.0
26	0.00π	51.3	0.49	13.1	13.1	1.24	23.9	−0.172	24.0	7.19	0.19	−0.38	−0.18	10.8
27	0.00π	49.8	0.51	16.1	8.5	1.25	23.8	−0.165	23.9	7.56	0.18	−0.24	−0.06	11.1
28	0.15π	50.3	0.50	8.5	16.6	1.35	23.8	−0.170	23.9	7.93	0.54	−0.12	0.42	12.7
29	0.15π	51.3	0.46	13.1	14.6	1.36	23.8	−0.180	23.9	7.56	0.66	−0.09	0.58	13.1
30	0.15π	50.3	0.47	16.6	10.0	1.42	23.7	−0.202	23.9	7.03	0.85	−0.05	0.80	13.6
31	0.22π	51.3	0.46	10.0	17.6	1.43	23.6	−0.198	23.8	7.22	0.91	−0.03	0.88	14.3
32	0.22π	51.3	0.49	13.1	13.1	1.52	23.6	−0.220	23.9	6.91	1.08	−0.02	1.07	14.7
33	0.23π	52.3	0.47	17.1	10.6	1.59	23.6	−0.239	23.9	6.65	1.15	−0.01	1.14	15.1

notice the major reduction and increase in the clockwise and counterclockwise loops, respectively, as t_d increases, leading to large improvements in $C_{w,net}$.

Trends similar to those for $C_{m,peak}$ are observed for the peak lift in Fig. 2c. Essentially no reduction in $C_{l,max}$ was observed for the $t_s = 0.5\pi$ case, because the flap deflection occurred after the LEV was shed into the wake, whereas for $t_s = 0\pi$, a $C_{l,max}$ of about 1.26 compared to 1.69 of a baseline airfoil, was observed; a reduction of about 25%, regardless of t_d. Furthermore, the peak lift, following the trend in the deflection angle at the moment of lift stall, decreased almost linearly with increasing t_d for $t_s = -0.5\pi$. In comparison to the $t_s = 0\pi$ control case, the $t_s = -0.5\pi$ case generated a larger peak lift for $t_d < 50\% f_o^{-1}$ and a smaller peak lift for $t_d \geq 50\% f_o^{-1}$. It is concluded that to minimize the reduction of the peak lift, a flap actuation initiated between the onset of flow reversal and the spillage of the LEV (i.e., $0\pi < t_s < 0.5\pi$) is needed. The behavior of the dynamic C_l–α loops at $t_s = 0\pi$ with different t_d is depicted in Fig. 3d. Also included in Figs. 3a and 3d are the static-airfoil data.

The underlying physics responsible for the observed decrease in lift and $C_{m,peak}$, as a result of the upward flap deflection, was mainly attributed to the increase in the pressure on the upper flap surface with a decrease, in particular, in the pressure on the lower surface. This pressure difference contributed to the drop and increment of the lift and nose-up pitching moment, respectively, during the actuation of the flap. This phenomenon, demonstrated in Fig. 4 using the $t_s = 0\pi$ with $t_d = 70\% f_o^{-1}$ control case, was more evident during the LEV formation and detachment (Figs. 4c and 4d) and during the during-stall (Fig. 4e) and pitch-down flow reattachment (Fig. 4f). Only a small variation in the C_p distributions was noticed at $\alpha_u = 16$ deg (i.e., below the static-stall angle α_{ss}) compared to the static-airfoil value at the same angle of attack (Fig. 4a). It is also of importance to note that for an oscillating airfoil with and without flap control, the unsteady boundary layer always remained attached for $\alpha_u > \alpha_{ss}$ (Fig. 4b), as a consequence of the boundary-layer improvement effects induced by the airfoil pitch-up motion, and the overall flow structure over the airfoil remained essentially unchanged.

The effectiveness of upward flap control was also evaluated based on the performance ratio of $|C_{l,max}/C_{m,peak}|$. Figure 2d shows no noticeable improvement over the baseline airfoil case for the $t_s = 0.5\pi$ case, proving that the flap deflection occurred too late in the oscillation cycle. Moreover, the earliest start time $t_s = -0.5\pi$ also showed no improvement until the duration exceeded $50\% f_o^{-1}$, at which point it began to increase. The highest $|C_{l,max}/C_{m,peak}|$ ratio was, however, generated by the $t_s = 0\pi$ control case, irrespective of duration. This revealed an advantage of longer duration for early start times (i.e., $t_s = -0.5\pi$–0π) that does not exist for later start times (i.e., $t_s = 0\pi$–0.5π). In addition, it further demonstrated that the best start time was in the vicinity of $t_s = 0\pi$; however, there was no preference whether the deflection was slightly earlier or slightly later.

Finally, the effect of t_d and t_s on the lift curve hysteresis C_H was also examined and is displayed in Fig. 2e. C_H is defined as the line integral of the C_l–α curve. In comparison to the baseline case, reductions in C_H result as the flap deflection begins earlier, with increased hysteresis occurring for the later start time. A consistent trend in t_d is not observed, with the $t_s = -0.5\pi$ case displaying a local minimum at $t_d = 52\% f_o^{-1}$, the $t_s = 0.5\pi$ case displaying a local maximum at $t_d = 52\% f_o^{-1}$ and the $t_s = 0\pi$ being roughly linear as a function of duration, falling in between the other two start times. This suggests a benefit from earlier start times and/or shorter durations. In summary, the results presented in Fig. 2 lead to the conclusion that a flap deflection duration $\geq 50\% f_o^{-1}$ which begins after $t_s = 0\pi$ but somewhat before $t_s = 0.5\pi$ leads to an optimum control of $C_{m,peak}$, $C_{w,net}$ and $|C_{l,max}/C_{m,peak}|$ with a small effect on $C_{l,max}$ and C_H.

B. Effect of R1

Based on the findings reported in Sec. III.A, the effect of the flap upward ramp rate (denoted by R1) on the critical aerodynamic values

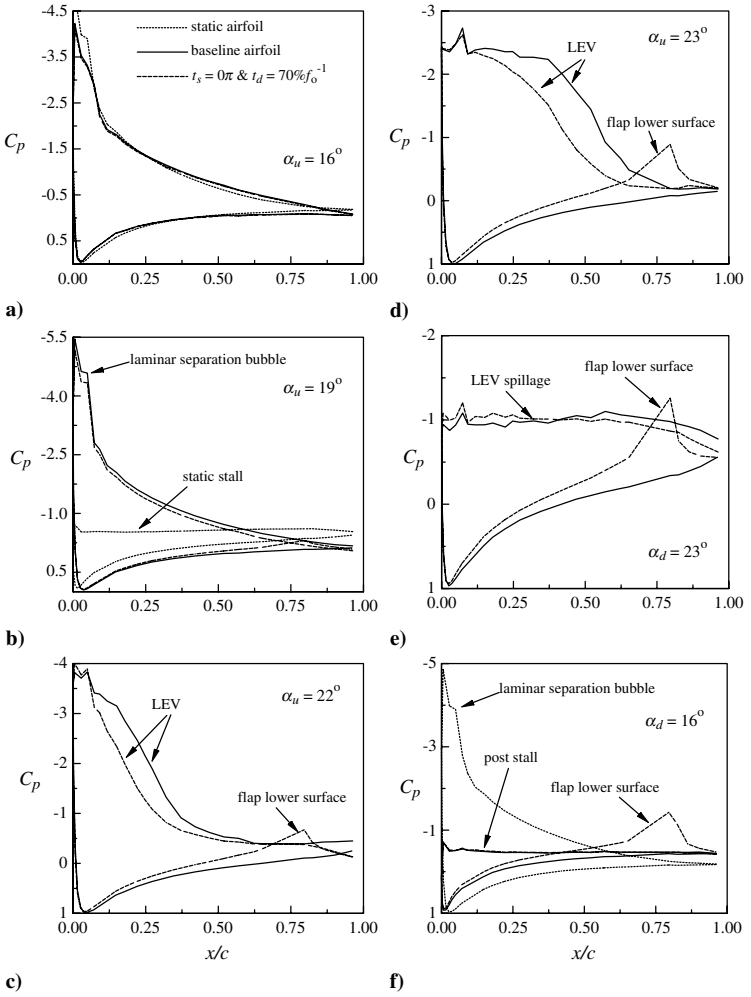

Fig. 4 Typical C_p distributions for $\delta_{max} = 16$ deg.

was investigated. The start time t_s was limited between 0π and 0.25π to ensure that the flap deflection began before the airfoil underwent moment stall at $\tau = 0.28\pi$ or $\alpha = 22.2$ deg during the upstroke, as suggested in Sec. III.A. The flap duration t_d was set to $51\%f_o^{-1}$ and $\delta_{\max}$ was set to 16 deg. Note that the portion of the oscillation cycle that the flap upward motion occupied, in percent, is denoted by t_{R1}. Therefore, a decrease in R1 is equivalent to an increase in t_{R1}, and vice versa. No reference to R2 is made because the downward slope of the flap deflection, in general, occurs during the downstroke of the airfoil oscillation when there are no significant events occurring over the airfoil. As such, the time allocated to the downward flap motion is of secondary importance and is determined as a result of first setting the values of t_d, t_{R1}, and t_{ss}.

Figure 5a shows that a greater reduction in the $C_{m,\text{peak}}$ was possible by increasing the upward ramp rate, regardless of the start time. The faster ramp rate allowed for a larger flap angle during moment stall, similar in effect to a reduction in start time. Furthermore, the start time was less effective at inducing a change in $C_{m,\text{peak}}$ at very fast or very slow ramp rates than at a medium ramp rate (i.e., approximately $t_{R1} = 25\%f_o^{-1}$). Figure 5a also reveals that to generate the largest improvement in $C_{m,\text{peak}}$ would therefore require an early start time with a fast ramp rate. It is also of interest to note that the fastest ramp rate generated a $C_{m,\text{peak}}$ less than that of a statically deflected flap ($C_{m,\text{peak}} = -0.151$ compared to -0.170; Table 1), which suggests the creation of an even stronger suction pressure on the lower side of the flap as a result of the quick flap motion. The present results also indicate that a reduction in the ramp rate, which is equivalent to an increase in t_{R1}, resulted in an increase in the aerodynamic damping which is nearly a linear function of t_{R1} (Fig. 5b). The slope of the relation between $C_{w,\text{net}}$ and t_{R1} decreased as the start time was delayed with a larger difference occurring between $t_s = 0.12\pi$ and 0.25π than between 0π and 0.12π. Note that all cases generate improvements in the aerodynamic damping except for $t_s = 0\pi$ at ramp times below 25% of the oscillation cycle, with the largest values of net work coefficient generated by a delayed start time and a slow ramp rate.

The reduction of the peak lift coefficient associated with the improvements in $C_{m,\text{peak}}$ and $C_{w,\text{net}}$ induced by an upward deflected flap was also examined. Figure 5c shows that as the ramp time t_{R1} was increased, the $C_{l,\max}$ was also increased (with values always below that of a baseline airfoil), regardless of the start time, an effect brought on by the delay in the full deflection of the flap and similar to the effect a delay in start time would have. As a result, the smallest loss in $C_{l,\max}$ is produced by a slow ramp rate, and can be enhanced by delaying the start time. Note, however, that the ramp rate control seems more effective at earlier start times and the start time is more effective at moderate ramp rates. Consequently, to minimize the loss in peak lift, a late start time in conjunction with a slow ramp rate is favorable. The effect of R1 on the performance ratio was also summarized in Fig. 5d and shows that all combinations of start time and ramp rate result in improvements in the $|C_{l,\max}/C_{m,\text{peak}}|$. Because of the slightly linear trend in the $C_{l,\max}$, the trend here is similar to that of $C_{m,\text{peak}}$ and therefore it is, in general, the earlier start times and the faster ramp rates that generate the higher ratios.

The effect of R1 on C_H is presented in Fig. 5e, displaying similar trends to those of the net work coefficient. C_H is an increasing nearly linear function of t_{R1}, with the slopes of the lines reducing slightly as the start time is delayed. Also, it is only at the fastest ramp rates for the earlier start times that the hysteresis is reduced compared to the baseline case. It is important to note, however, the source of the

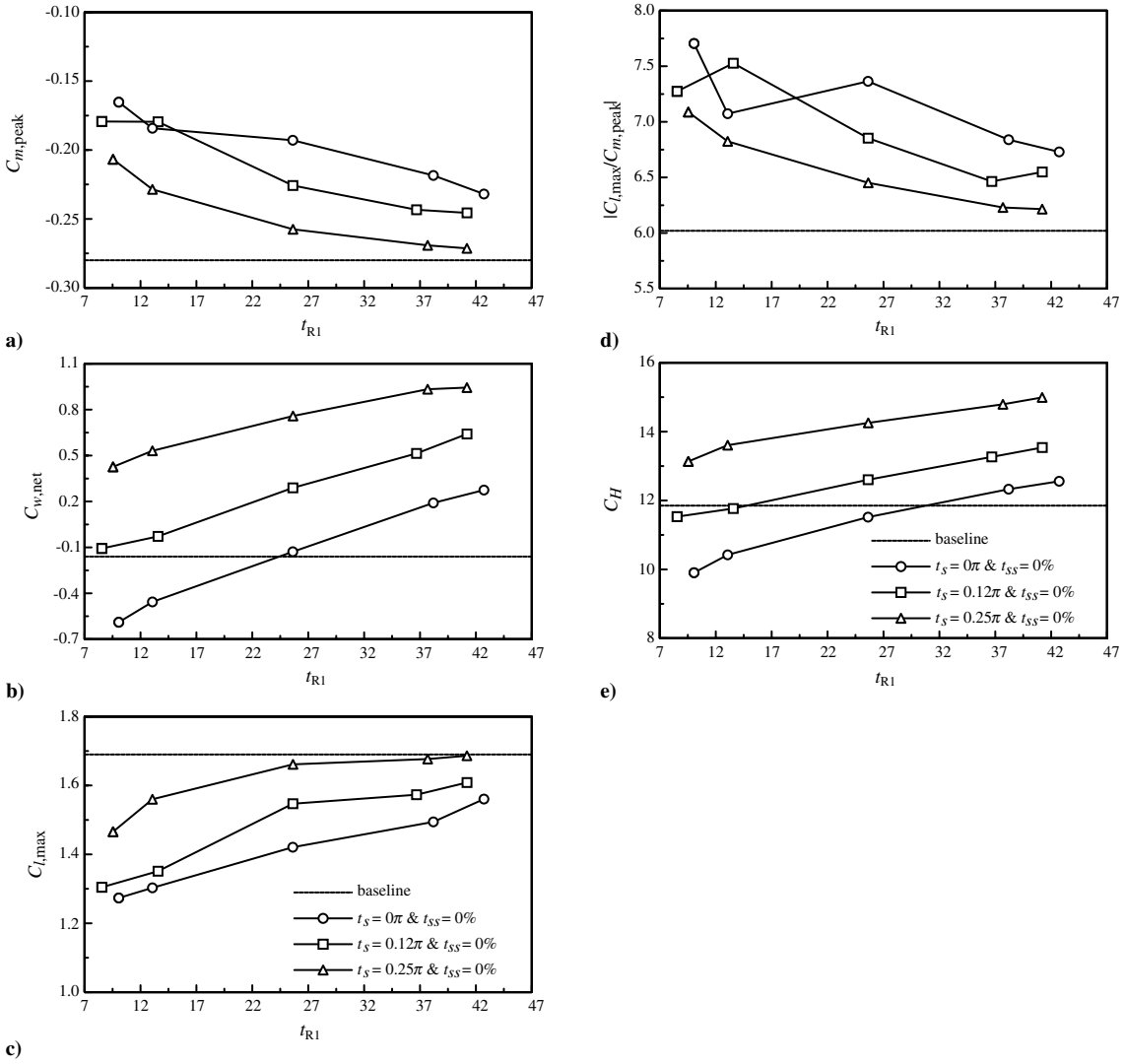

Fig. 5 Critical aerodynamic values for various t_{R1}.

increased/decreased hysteresis. A reduction of lift during the upstroke contributes to a decrease in C_l hysteresis, whereas during the downstroke the contribution would be positive. It is, therefore, the proportion of flap deflection duration during the upstroke to that during the downstroke that determines whether the hysteresis increases, decreases, or remains roughly unchanged. Note, however, that this is not the ideal case, which would be to reduce hysteresis by increasing the lift during the downstroke portion of the oscillation cycle requiring a negative (downwards) deflection of the flap during the downstroke.

An analysis was also done to determine whether a steady-state portion t_{ss} after the flap upwards motion is advantageous. Table 1 shows that comparing two cases at fixed $t_s = 0\pi$ and $t_{R1} = 13\% f_o^{-1}$: the first with $t_{ss} = 0\% f_o^{-1}$ (case 11) and the second with $t_{ss} = 25\% f_o^{-1}$ (case 26), it is clear there exists contradictory requirements. Introducing the steady-state portion improves the $C_{m,\text{peak}}$ and $|C_{l,\max}/C_{m,\text{peak}}|$ to a small degree (39 and 19% vs 34 and 17%), improves the $C_{w,\text{net}}$ to a large degree (-18 vs -192%), but reduces the $C_{l,\max}$ (27 vs 23%) and does not improve C_H as much (9 vs 12%). Although most differences are small, the significant improvement in the net work coefficient suggests that, in fact, having a steady-state portion in between the flap upward and downward deflections is advantageous. Note, however, that as a result of the steady-state portion of the flap motion, the flap upwards ramp rate is required to increase so as to keep t_d constant. The advantages of having a slower ramp rate could therefore not be fully used and it should be noted that the improvements brought on by a slower ramp rate are more significant than those brought on by having $t_{ss} \neq 0\%$. In light of this, it is therefore recommended to keep t_{ss} small with any time spent in a steady-state motion being removed from the time spent returning to an undeflected position (i.e., decreasing t_{R2}).

From the preceding paragraphs, it can be concluded that the critical aerodynamic values can be subdivided into two categories: those whose performance are improved at early start times and fast ramp rates, which are $C_{m,\text{peak}}$, $|C_{l,\max}/C_{m,\text{peak}}|$, and C_H, and those whose performance are improved at late start times and slow ramp rates, which are $C_{l,\max}$ and $C_{w,\text{net}}$. This poses the dilemma of determining the best range of start times and ramp rates. In fact, there can be no best range as the requirements are contradictory. We can examine this, however, by comparing two cases: the first with $t_s = 0\pi$ and $t_{R1} = 25\% f_o^{-1}$ (case 12) and the second with $t_s = 0.25\pi$ and $t_{R1} = 13\% f_o^{-1}$ (case 21). These two cases are chosen because they both achieve their peak deflections at the same time, near the instant that the peak negative pitching moment is achieved. The first case outperforms the second case in terms of $C_{m,\text{peak}}$ (31 vs 18%), $|C_{l,\max}/C_{m,\text{peak}}|$ (22 vs 13%) and C_H (3 vs -15%), whereas the second case is superior in terms of $C_{l,\max}$ (-7 vs -16%) and $C_{w,\text{net}}$ (0.53 vs -0.13). A TEF control case falling somewhere in between the aforementioned two cases, such as $t_s = 0.12\pi$ and $t_{R1} = 19\% f_o^{-1}$, would result in a compromise in performance where $C_{m,\text{peak}}$, $|C_{l,\max}/C_{m,\text{peak}}|$, and $C_{w,\text{net}}$ are still very much improved over the baseline case and where the reduction in $C_{l,\max}$ and increase in C_H are not too severe.

IV. Conclusions

The effectiveness of upward flap motions actuated at various start times, flap deflection rates, steady-state periods, and total durations, with the flap deflection fixed at 16 deg or $67\%\alpha_{\max}$, on the dynamic pitching moment of an oscillating airfoil was investigated. The results showed that 1) the maximum reduction in the nose-down pitching moment required a $t_s \approx 0\pi$ with a quick upward flap ramp rate corresponding to $t_{R1} \approx 10\% f_o^{-1}$; 2) the largest torsional damping factor was produced by a $t_d \approx 50\% f_o^{-1}$, $t_s \approx 0.5\pi$, and slow $t_{R1} \approx 40\% f_o^{-1}$; 3) the maximum lift was highly sensitive to t_s and t_{R1} calling for a delayed start time and/or slow ramp rate to minimize its reduction; 4) the performance ratio ($|C_{l,\max}/C_{m,\text{peak}}|$) was highest for $t_d > 50\% f_o^{-1}$, $t_s \approx 0\pi$, and $t_{R1} \approx 10\% f_o^{-1}$; and 5) the lift curve hysteresis was most reduced for $t_s \approx -0.5\pi$, $t_d \approx 50\% f_o^{-1}$, and $t_{R1} \approx 10\% f_o^{-1}$. Furthermore, it was found that having a steady-state portion as part of the flap motion is advantageous; however, it should be small (i.e., $t_{ss}/t_d < 50\%$) so as not to impose an overly fast upward flap motion to the detriment of $C_{w,\text{net}}$. It is also evident that the various criteria used to evaluate the different control cases could have opposing requirements, making the creation of an optimum flap motion unachievable. A compromise can, however, be formulated that results in significant improvements. This would involve a $t_d \approx 50\% f_o^{-1}$, $t_s \approx 0.12\pi$, $t_{R1} \approx 19\% f_o^{-1}$, and $t_{ss}/t_d \approx 35\%$.

Acknowledgment

This work was supported by the Natural Science and Engineering Research Council (NSERC) of Canada.

References

[1] McCroskey, W. J., "Unsteady Airfoils," *Annual Review of Fluid Mechanics*, Vol. 14, Jan. 1982, pp. 285–311.

[2] Lee, T., and Gerontakos, P., "Investigation of Flow over an Oscillating Airfoil," *Journal of Fluid Mechanics*, Vol. 512, Aug. 2004, pp. 313–341.

[3] Rennie, R., and Jumper, E. J., "Experimental Measurements of Dynamic Control Surface Effectiveness," *Journal of Aircraft*, Vol. 33, No. 5, 1996, pp. 880–887.

[4] Vipperman, J. S., Clark, R. L., Conner, M., and Dowell, E. H., "Experimental Active Control of a Typical Section Using a Trailing-Edge Flap," *Journal of Aircraft*, Vol. 35, No. 2, 1998, pp. 224–229.

[5] Ekaterinaris, J. A., "Numerical Investigations of Dynamic Stall Active Control for Incompressible and Compressible Flows," *Journal of Aircraft*, Vol. 39, No. 1, 2002, pp. 71–78.

[6] Feszty, D., Gillies, E. A., and Vezza, M., "Alleviation of Airfoil Dynamic Stall Moments via Trailing-Edge-Flap Flow Control," *AIAA Journal*, Vol. 42, No. 1, 2004, pp. 17–25.

[7] Gerontakos, P., and Lee, T., "Dynamic Stall Flow Control via a Trailing-Edge Flap," *AIAA Journal*, Vol. 44, No. 3, 2006, pp. 469–480.

[8] Smith, B. L., and Glezer, A., "The Formation and Evolution of Synthetic Jets," *Physics of Fluids*, Vol. 10, No. 9, 1998, pp. 2281–2297.

[9] Greenblatt, D., and Wygnanski, I., "Dynamic Stall Control by Periodic Excitation, Part 1: NACA 0015 Parametric Study," *Journal of Aircraft*, Vol. 38, No. 3, 2001, pp. 430–438.

[10] Karim, M. A., and Acharya, M., "Suppression of Dynamic-Stall Vortices over Pitching Airfoils by Leading-Edge Suction," *AIAA Journal*, Vol. 32, No. 8, 1994, pp. 1647–1655.

[11] Chandrasekhara, M. S., Wilder, M. C., and Carr, L. W., "Unsteady Stall Control Using Dynamically Deforming Airfoils," *AIAA Journal*, Vol. 36, No. 10, 1998, pp. 1792–1800.

W. Ng
Associate Editor